



CHORUS

This is the accepted manuscript made available via CHORUS. The article has been published as:

Adsorption-induced shape transitions in bistable nanopores with atomically thin walls

Oleg E. Shklyaev, Milton W. Cole, and Vincent H. Crespi

Phys. Rev. E **95**, 012804 — Published 13 January 2017

DOI: [10.1103/PhysRevE.95.012804](https://doi.org/10.1103/PhysRevE.95.012804)

Adsorption-induced shape transitions in bistable nanopores with atomically thin walls

Oleg E. Shklyaeu, Milton W. Cole, Vincent H. Crespi

Department of Physics, The Pennsylvania State University, University Park, PA, 16802-6300, USA

(Dated: December 15, 2016)

Atomically thin cylindrical nanopores can change shape in response to physically adsorbed gas inside. Coupled to a gas reservoir, an initially collapsed pore can expand to allow the adsorbed gas to form concentric shells on the inner part of the pore, driven by adsorption energetics, not gas pressure. A lattice gas model describes the evolution of the pore/nanotube shape and adsorbed gas as a function of gas chemical potential at zero temperature. We found that narrow-enough tubes are always expanded and gas inside adsorbs in sequences of concentric shells as the gas chemical potential increases. Wider tubes, which are collapsed without gas, can expand with one or more concentric shells adsorbed on the inner surface of the expanded region.

PACS numbers: 68.43.-h, 61.48.De, 64.70.Nd

I. INTRODUCTION

The flexible, mechanically strong nature of certain atomically thin, two-dimensional materials can promote degrees of freedom previously thought of as simply thermodynamic constraints – the surface area and volume – into fully dynamical variables. Consider, for example, a two-dimensional material rolled into a cylindrical geometry, i.e. a nanotube. The nanopore defined by the cylinder’s interior can adsorb inert gases. At a static level, the nanotube geometry just accentuates the gas-substrate interaction by increasing coordination number, thus facilitating the formation of concentric shells of adsorbed gases¹. But if the pore wall is allowed to express dynamics, then new modes of response can emerge, particularly when the wall enters a mechanically nonlinear regime. Large-radius nanotubes from carbon, boron nitride, or other two-dimensional materials are mechanically bistable^{2–8} with both circular/expanded and flattened/collapsed cross-sectional shapes. The flattened shape is favored at sufficiently large radii, where the elastic energy cost of collapse is overpowered by the interfacial energy gain of placing the opposing interior faces into contact. Not only does the cross-sectional shape of the system affect the behavior of the adsorbed gas (by defining the character of the adsorption sites), but the ambient gas also affects the cross-sectional shape (by changing the interfacial energies). The gas degrees of freedom interact with the container degrees of freedom on an equal footing and phase transitions in the gas should be able to control the shape of their nanoscale container.

Recent investigations have studied the response of the partially collapsed tube depicted in Fig. 1 to changes in the temperature⁹, voltage¹⁰, or the strength of the Lennard-Jones interaction¹¹, and used these behaviors to design nano-scale motors, generators, and pumps of heat or fluid¹⁰. Coupling to a gas reservoir provides another means of control, with interior gas expected to generically favor expansion. Previously studies of the expansion of a slit pore¹² or narrow nanotube¹³ due to gas uptake were limited to small, linear deformations. Here we explore shape transitions with large radial displacements that convert a low-symmetry collapsed structure

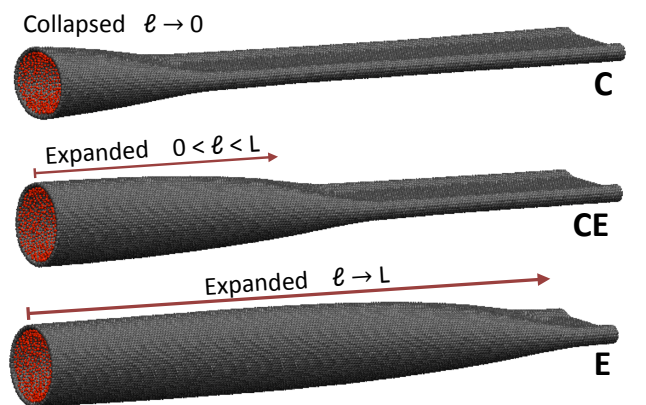


FIG. 1: (Color online) Equilibrium shapes of a partially collapsed tube of length L with gas inside. Left and right ends are held open and closed by boundary conditions. Characterizing the tube shape by the length ℓ of the expanded region, the following configurations are considered: collapsed with $\ell = 0$ (**C**, top); mixed collapsed-expanded with $0 \leq \ell \leq L$ (**CE**, middle); and expanded with $\ell = L$ (**E**, bottom).

to a high-symmetry circular cross-section in response to gas adsorption, facilitated by boundary conditions that pin one end of the tube open (as could be imposed by a rigid endcap) and the other end closed (as could be imposed by mechanical compression)¹⁴.

We investigate equilibrium configurations of atomically thin nanotubes with adsorbed gas at zero temperature by minimizing the full grand free energy, including contributions from the tube wall, gas-gas interactions, and gas-wall interactions. The inert gases considered in this work exhibit strong wetting interactions with the walls of carbon nanotubes^{15–17}. The wall of the tube is described within a quasi-one-dimensional approximation¹⁰ in which the elastic energy is modeled as a sum of two contributions that are linearly proportional to the lengths of the expanded and collapsed regions (see Fig. 1). The proportionality coefficients, representing the energies per unit of length of the expanded and collapsed cross-sections, were

computed using atomistic simulations as described in the Appendix. As mentioned above, in our model one end of the tube is taken to be pinned in the inflated state and the other end pinned in the collapsed state, so that a transition region between collapse and expansion is always present and merely shifts along the tube axis as the tube changes state. Thus the energy of the transition region itself can be neglected for the purposes of determining equilibrium configurations, since it cancels out of all free energy comparisons. (Subtle effects when the transition region interacts with a boundary condition can also be neglected when the tube is much longer than the transition region). The other contribution to the grand free energy comes from the absorbed gas, which is treated in the lattice-gas approximation for condensation inside the tube^{1,18}. Lattice gas atoms interact with both the tube wall and nearest-neighbor gas atoms, and reside either within the tightly confining bulbs at either edge of the collapsed cross-section (which can accommodate just a single close-packed shell of adsorbed gas at the low temperatures considered here) or within the more roomy interior of the expanded cross-section, as depicted in Fig. 2. The equilibrium configuration of the system for a fixed chemical potential and tube radius will be found by minimizing the grand free energy (incorporating the elastic energy of the tube wall and the energy of the absorbed lattice gas) with respect to relative lengths of the expanded and collapsed regions of the tube and the number of the absorbed gas shells in the expanded and collapsed regions.

To denote configurations of the system that combine the shape of the tube wall with the structures of the adsorbed gas atoms, we develop the following nomenclature. We use a letter **C** or **E** to convey the cross-sectional shape, followed by an integer to represent the number of adsorbed layers of gas. A collapsed tube without gas (**C0**) competes against one with a single shell of gas adsorbed in the bulbs (**C1**), a mixed collapsed-expanded tube with one shell in the bulbs and m shells absorbed in the expanded region (**C1Em**), and an expanded tube without gas (**E0**) or with m shells of adsorbed gas (**Em**). Any gas adsorbed onto the outer surface does not couple strongly to the wall geometry, since the accessible surface area on the outside is essentially unchanged by the shape transition.

II. ZERO-TEMPERATURE ANALYSIS

Consider adsorption of an inert gas at $T = 0$ inside a nanotube that has atomically thin walls and whose opposite ends are pinned open and closed, as in Fig. 1. Characterizing the tube wall geometry by the radius R and the length ℓ of the expanded region, and assuming appropriate structure of the adsorbed gas shells, we search for equilibrium configurations of such a system by minimizing the grand free energy. The energy of the tube filled with gas is approximated by three contributions: the energy of the tube wall calculated using a quasi-

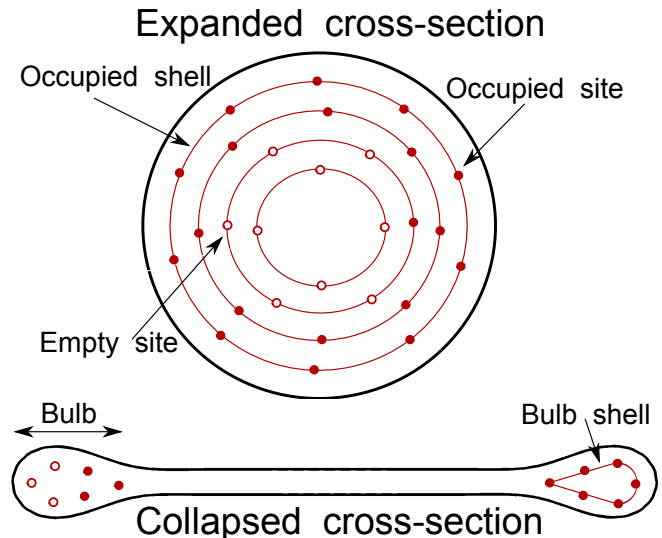


FIG. 2: (Color online) Allowed locations for gas atoms within the lattice gas model for both expanded and collapsed shapes. Red lines show shells.

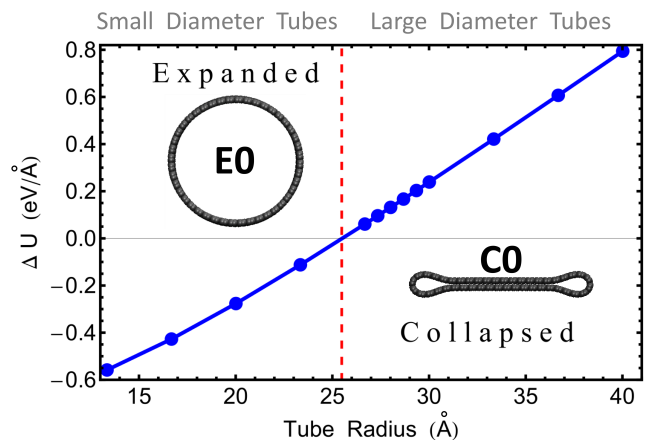


FIG. 3: (Color online) The difference in energy per unit length $\Delta U(R) = U_+ - U_-$ between expanded (U_+) and collapsed (U_-) configurations for an empty tube. The expanded shape minimizes the energy for tubes with radii below the vertical dashed line at R_c ; the collapsed shape minimizes for radii above. The two shapes provide different accessible surface areas for atoms adsorbed onto the inner surface. Note that both shapes are metastable at large-enough radius.

one-dimensional model¹⁰ with parameters determined by atomistic simulations; the interaction energy between the adsorbed gas atoms determined by a lattice-gas model in which the structure of the adsorbed gas shells depends on the tube's cross-sectional shape; and the interaction energy between carbon atoms of the tube wall and the adsorbed gas atoms, also calculated within the lattice gas model.

In a quasi-one-dimensional approximation¹⁰, the energy of a gas-free tube of length L is a function $U(\ell) =$

$LU_- + \ell\Delta U$ of length ℓ with $\Delta U = U_o - U_-$ being the difference in the energy per unit length of expanded (U_o) and collapsed (U_-) regions. To parametrize this model, the potential energies $U_o(R)$ and $U_-(R)$ for uniformly expanded and collapsed tubes of different radii were computed using molecular dynamics simulations within the LAMMPS package¹⁹ with the bonded and non-bonded inter-carbon interactions modeled by the adaptive intermolecular reactive empirical bond order (AIREBO) potential²⁰ (see Appendix). The resulting radius dependence of $\Delta U(R)$ for one archetypal system, a pure-carbon sp^2 pore wall of armchair geometry, is shown in Fig. 3; (similar phenomena should occur for other atomically thin cylinders, e.g. hexagonal boron nitride). The expanded shape wins when $R < R_t$, marked by a dashed red line. These narrow tubes are fully expanded, as shown on the left inset in Fig. 3, even without interior gas. Wider tubes in the absence of interior gas are most stable when collapsed. These two geometries are shown in Fig. 3. Tubes with radii greater than $R_t \approx 25 \text{ \AA}$ can be grown by chemical vapor deposition with a tailored catalyst²¹. (Note here that we quote the energies of the expanded and collapsed states as per unit length of the tube, rather than as an energy per atom of the tube wall: this is the natural choice of units for the quasi-one-dimensional treatment and also the natural language for describing any nucleation barriers against transitions between expanded and collapsed states, since they would depend on the characteristic axial length of a transition region).

To construct the lattice gas model^{1,18}, the structure of the adsorbed gas shells, their number, and the inter-shell distances have to be specified in the expanded and collapsed regions (Fig. 2). To determine these, we model gas-gas interactions by a Lennard-Jones potential $\phi(r) = 4\epsilon[(\sigma/r)^{12} - (\sigma/r)^6]$. The gas-tube interactions are described by integrating the Lennard-Jones potential over an infinite tube²²:

$$v(r, R) = 3\pi\theta\epsilon\sigma^2 \left[\frac{21}{32} \left(\frac{\sigma}{R}\right)^{10} M_{11}(x) - \left(\frac{\sigma}{R}\right)^4 M_5(x) \right] \quad (1)$$

Here $x = r/R$ measures the dimensionless distance of the gas atom from the central axis, $\theta = 0.38 \text{ \AA}^{-2}$ is the atomic surface density of the wall, and the parameters $\epsilon = \sqrt{\epsilon_W \epsilon_G}$ and $\sigma = \frac{1}{2}(\sigma_W + \sigma_G)$ come from the conventional combining rules for interactions between a gas atom $G = \text{He, H}_2, \text{Ar, Ne, Kr, and Xe}$ and a wall atom W . $M_{11}(x)$ and $M_5(x)$ are elliptic integrals. The error in extending the integral to infinity is small if $R, r \ll L, \ell$, which is typically the case. Wall parameters ϵ_W and σ_W for an sp^2 carbon wall²³ and the parameters ϵ_G and σ_G for He, Ne, Ar, Kr, and Xe²² and H_2 ²⁴ are taken from the cited sources.

The expanded region can hold M concentric shells of adsorbed gas. We assume that the shells have a close-packed structure (consistent with finite temperature atomistic simulations discussed in Appendix) and are separated by a distance $\delta = 2^{1/6}\sigma$ with the shell closest to the tube wall located at the distance minimizing the gas-wall potential, $\frac{\partial v(r, R)}{\partial r} = 0$. All shells interact with the tube

wall at the appropriate separation distance, in addition to interactions with $z_\perp = 6$ nearest neighbors in the same shell and $z_\parallel = 3$ neighbors in adjacent shells (adjusted for shell curvature as described below). The gas parameters ϵ and σ and the tube radius together determine M .

The detailed structure of the gas shell in the bulb regions is less obvious because atoms and molecules adsorbing into pores whose diameter is comparable to the sizes of the adsorbed species can assume varied packing geometries, as is observed for fullerenes²⁵, diamondoids²⁶, and organic molecules²⁷ within nanotubes. To determine a type of packing most suitable for our situation, we used molecular dynamics to simulate helium filling a nanotube at 10 K. The results presented in the Appendix reveal that the radius of the tube wall forming the bulb is $r \approx 5 \text{ \AA}$ (see Fig.10) and that the gas adsorbs into a single close-packed shell in the bulb that is separated from the tube wall by $\sim 3 \text{ \AA}$ (see Fig. 9b,c). More complex staggered or helical shell geometries are not observed. The diameter $\sim 4 \text{ \AA}$ of the first shell leaves no room for a second shell: the formation of a second shell would require a substantial elastic deformation of the bulb wall, which is unfavorable at low temperatures. For comparison, regular inflated carbon nanotubes filled with helium only form a second (i.e. axial) shell when the tube radius is $\geq 6 \text{ \AA}$ ²⁸, which is significantly larger than the bulbs observed in our simulations. Thus we assume that the bulbs are occupied by a single close-packed shell. Later, we will discuss possible effects of different packing geometries in the bulbs on the observed phase behavior. For simplicity, we assume that the gas atoms in the bulb see an adsorption potential similar to that of tube 5 \AA in radius, but we model the geometry of the adsorbed layer in the bulb as a semicircle at the appropriate equilibrium radius plus two straight segments of length 9 \AA , as shown in Fig. 2. These dimensions approximate the geometry of the bulb region obtained from atomistic simulations of the cross-sectional shape; the essential results are not anticipated to be sensitive to the details of this geometrical approximation. Note that the bulb regions are much less capacious than the corresponding inflated regions of the same tube, thus the relative phase stability of the various inflated and collapsed states discussed below is affected only weakly by assumptions about the detailed packing geometry in the bulbs.

The $T = 0$ equilibrium state of the system is a function of gas chemical potential μ and the tube radius. The grand free energy of the tube of length ℓ with zero or m adsorbed shells in the expanded region and zero or one shell m_- in each bulb is

$$\Omega(\ell, m, m_-, \mu) = \ell \left(\Delta U + \sum_{j=1}^m n_j \left[\epsilon \left(\frac{z_\parallel}{2} + \frac{n_{j+1}}{n_j} z_\perp \right) + v_j - \mu \right] \right) + (L - \ell) n_- \left[\frac{\epsilon z_\parallel}{2} + v_- - \mu \right] m_-, \quad (2)$$

where $n_j = \frac{2\pi r_j}{a_0}$ is the number of lattice gas sites per

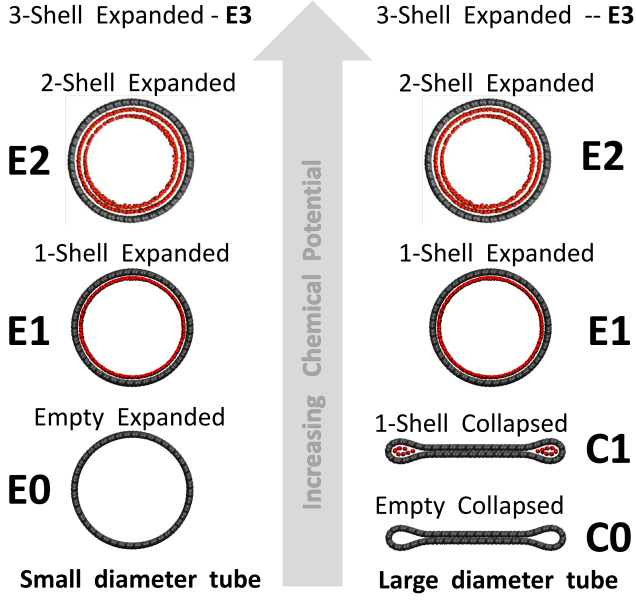


FIG. 4: (Color online) Schematic showing two different scenarios for the evolution in gas coverage as μ increases. Narrow tubes simply add successive layers to the inner surface of the expanded cross-section, following the sequence $\mathbf{E0} \rightarrow \mathbf{E1} \rightarrow \mathbf{E2} \rightarrow \dots \rightarrow \mathbf{Em}$. Wider tubes adsorb first in the bulbs; further gas adsorption then forces the pore open along the sequence $\mathbf{C0} \rightarrow \mathbf{C1} \rightarrow \mathbf{E1} \rightarrow \mathbf{E2} \rightarrow \dots \rightarrow \mathbf{Em}$.

unit axial length in the j^{th} shell of the expanded region, v_j is the value of the wall potential from Eqn. 1 in the j^{th} shell at radius r_j , and n_- and v_- are the corresponding quantities for the bulbs. The curvature factor $\frac{n_{j+1}}{n_j} = \frac{r_{j+1}}{r_j} < 1$ accounts for the reduction of nearest neighbors in the innerward adjacent shell due to its smaller radius. a_0 is the area per gas atom in an adsorbed layer. The dependence of $\Omega(\ell, m, m_-, \mu)$ on tube radius is implicit in the dependences on r_j , n_j , and v_j . For a given tube radius and chemical potential, the $T = 0$ isotherms are determined by minimizing $\Omega(\ell, m, m_-, \mu)$ with respect to the length ℓ of expanded region, the number of shells m in that region, and optional occupation of the bulbs m_- and comparing to the empty tube with $U(\ell) = \ell\Delta U$.

Narrow tubes with $R < R_t$ have the simplest behavior since they are always fully expanded, with $\ell = L$. The first adsorbed shell forms when $\Omega(L, 1, 0, \mu) < \Omega(L, 0, 0, \mu) = L\Delta U$,

$$\mu = \epsilon \frac{z_{\parallel}}{2} + v_1, \quad \mathbf{E0} \rightarrow \mathbf{E1}. \quad (3)$$

The $(m+1)^{\text{th}}$ shell forms on top of the m^{th} shell when $\Omega(L, m+1, 0, \mu) < \Omega(L, m, 0, \mu)$,

$$\mu = \epsilon \left(\frac{z_{\parallel}}{2} + z_{\perp} \right) + v_{m+1}, \quad \mathbf{Em} \rightarrow \mathbf{E(m+1)}. \quad (4)$$

This sequence of shell-filling transitions is shown schematically in the left column of Fig. 4.

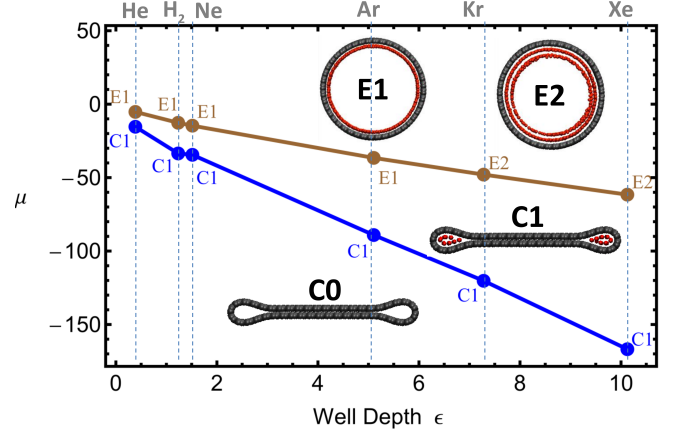


FIG. 5: (Color online) The shape of tube of radius 26.7 \AA as a function of the gas chemical potential μ and the gas-gas interaction strength ϵ . As μ increases, the bulbs of the initially empty collapsed tube fill with gas at the lower blue line. The tube then expands into a state with one or two shells of adsorbed gas. Further increase of μ yields additional concentric shells. ϵ and μ are given in units of ϵ_W .

Wider tubes start collapsed, but can expand upon gas adsorption, as shown in the right column of Fig. 4. The first adsorbed shell forms in the bulbs of the empty collapsed tube when $\Omega(0, 0, 1, \mu) < U(0) = 0$,

$$\mu > \epsilon \frac{z_{\parallel}}{2} + v_-, \quad \mathbf{C0} \rightarrow \mathbf{C1}. \quad (5)$$

Although the coordination of a gas atom to the wall is higher in the tightly curved bulbs, the number n_- of adsorbed atoms per unit length in the collapsed state is much smaller than the number n_j in each shell of the expanded state. Therefore the system can minimize its free energy at higher μ by expanding and forming shells in the expanded region. The one-shell expanded phase is favored relative to the one-shell collapsed phase when $\Omega(L, 1, 0, \mu) < \Omega(0, 0, 1, \mu)$,

$$\mu > \frac{\Delta U + n_1 \left(\frac{\epsilon z_{\parallel}}{2} + v_1 \right) - n_- \left(\frac{\epsilon z_{\parallel}}{2} + v_- \right)}{n_1 - n_-}, \quad (6)$$

$$\mathbf{C1} \rightarrow \mathbf{E1}.$$

At this threshold, the system transitions from fully collapsed at $\ell = 0$ to fully expanded with $\ell = L$ and one adsorbed shell.

Since wider tubes more strongly favor collapse, they require multiple shells to force expansion and transform directly into a multiple-shell structure \mathbf{Em} . The m -shell phase in the expanded state is favored relative to the one-shell phase in the collapsed state when $\Omega(L, m, 0, \mu) <$

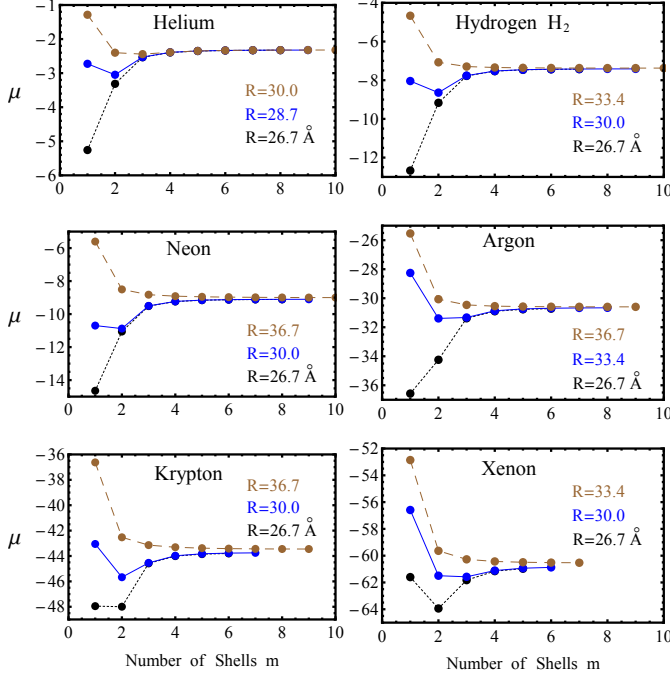


FIG. 6: (Color online) Chemical potential corresponding to a given number of adsorbed shells in the expanded tube for various adsorbed gases and tube radii. The shell thicknesses on the negative slope to the left of minimal μ_m are skipped, and those systems expanded directly into a state with multiple shells. μ is given in units of ϵ_C .

$\Omega(0, 0, 1, \mu)$:

$$\mu > \frac{\Delta U + \sum_{j=1}^m n_j \left[\epsilon \left(\frac{z_{\parallel}}{2} + \frac{n_{j+1}}{n_j} z_{\perp} \right) + v_j \right] - n_- \left(\frac{\epsilon z_{\parallel}}{2} + v_- \right)}{\sum_{j=1}^m n_j - n_-} \quad \text{C1} \rightarrow \mathbf{E}m. \quad (7)$$

Fig. 5 shows the tube configuration as a function of the gas-gas interaction strength ϵ and the chemical potential μ for a representative radius $R > R_t$. The dots represent ϵ and μ for He, H₂, Ne, Ar, Kr, and Xe. As μ increases, a first shell absorbs $\mathbf{C0} \rightarrow \mathbf{C1}$ inside the bulbs of the empty collapsed tube across the blue line defined by Eqn. 5. The collapsed tube inflates $\mathbf{C1} \rightarrow \mathbf{E}m$ at the brown line defined by Eqn. 7. For He, H₂, Ne, and Ar a single shell absorbs inside the expanded region during inflation, whereas Kr and Xe expand into a state with two shells. Further increase in μ deposits additional concentric shells. Thus a phase boundary exists between Ar and Kr where the shell thickness at the moment of expansion increases from one to two.

Combining the expansion process $\mathbf{C1} \rightarrow \mathbf{E}m$ with the sequential addition of shells to an already-expanded tube $\mathbf{E}m \rightarrow \mathbf{E}(m+1)$, we obtain a full phase diagram as a function of gas chemical potential. Eqn. (7) identifies the number of shells m in the expanded region that minimizes μ_m at $\mathbf{C1} \rightarrow \mathbf{E}m$. After expansion, Eqn. (4) yields the

values μ_{m+1}, \dots, μ_M at which the remaining $M - m$ inner shells form: the first m values μ_1, \dots, μ_m are monotonically decreasing, so they are unstable against the minimal value μ_m . These transitions are shown in Fig. 6 for various gases and representative tube radii. Consider the case of helium. For $R = 26.7 \text{ \AA}$, the sequence μ_1, μ_2, \dots is monotonically increasing, so expansion occurs at $m = 1$. For a slightly wider tube with $R = 28.7 \text{ \AA}$, μ_1 is larger than μ_2 , so the system transitions from the one-shell collapsed state $\mathbf{C1}$ into a double-shell expanded phase $\mathbf{E2}$ at μ_2 . Larger radii carry this trend further, until at large-enough radius the gas absorbs into all shells simultaneously at μ_M – the maximal possible shell number – in a process of simultaneous pore opening and capillary condensation. In this case μ_m is a monotonically decreasing function of m so that $\mu_{m+1} \leq \mu_m$. Fig. 7 shows the thickness of the adsorbed shell at the transition to the expanded state across a broad range of tube radii and gas-gas interaction strengths. The large jump in initial layer thickness indicated by the transition to boldface font marks the onset of capillary condensation. Unlike traditional capillary condensation into a rigid pore, this phenomenon involves two simultaneous transitions: one in pore shape and another in adsorbate configuration. Since the bulbs are effectively already capillary condensed at a single layer, this can also be thought of as a transition between two different capillary condensed states, with different pore shapes.

Instead of working at fixed chemical potential, we can instead minimize the total energy at fixed number of gas atoms $N = (L - \ell)n_- + \ell \sum_{j=1}^m n_j$ inside the tube, which is the appropriate constraints for fully encapsulated gas. A system with fixed N remains collapsed below a threshold $N_1 = (L - \ell)n_-$, presents a mixed collapsed/expanded state ($\mathbf{C1E}m$) from $N_1 < N < N_2$, and fully expands for $N_2 = \sum_{j=1}^m n_j$. The number of shells m formed at $\mathbf{C1} \rightarrow \mathbf{E}m$ in Fig. 7 now corresponds to transitions $\mathbf{C1E}m \rightarrow \mathbf{E}m$ where the partially inflated state may have a variable number of shells as it works its way towards the fully expanded state.

We expect that more complex staggered or helical gas shell structures in the bulbs, as mentioned previously for adsorption into narrow pores, will not change the main sequence of transitions in which the bulbs (with higher carbon coordination number) are populated first and then the expanded part is populated after the expansion of the tube. An alternative packing could have a different number of in-shell z_{\parallel} and out-of-shell z_{\perp} neighbors, which could shift the value of chemical potential corresponding to the bulb-filling $\mathbf{C0} \rightarrow \mathbf{C1,2}$ (2 is for axial shell) and tube-expansion $\mathbf{C2} \rightarrow \mathbf{E}m$ transitions. However, these shifts will be small, since the number n_j of gas atoms in the expanded region is much larger than that the number n_- in the collapsed region: i.e. the adsorption energetics in the inflated region dominates the transition $\mathbf{C2} \rightarrow \mathbf{E}m$ (6). In general, the relatively small capacity of the bulbs means that the details of bulb packing will only weakly affect the overall phase behavior of the system.

For concreteness, the discussion above describes the

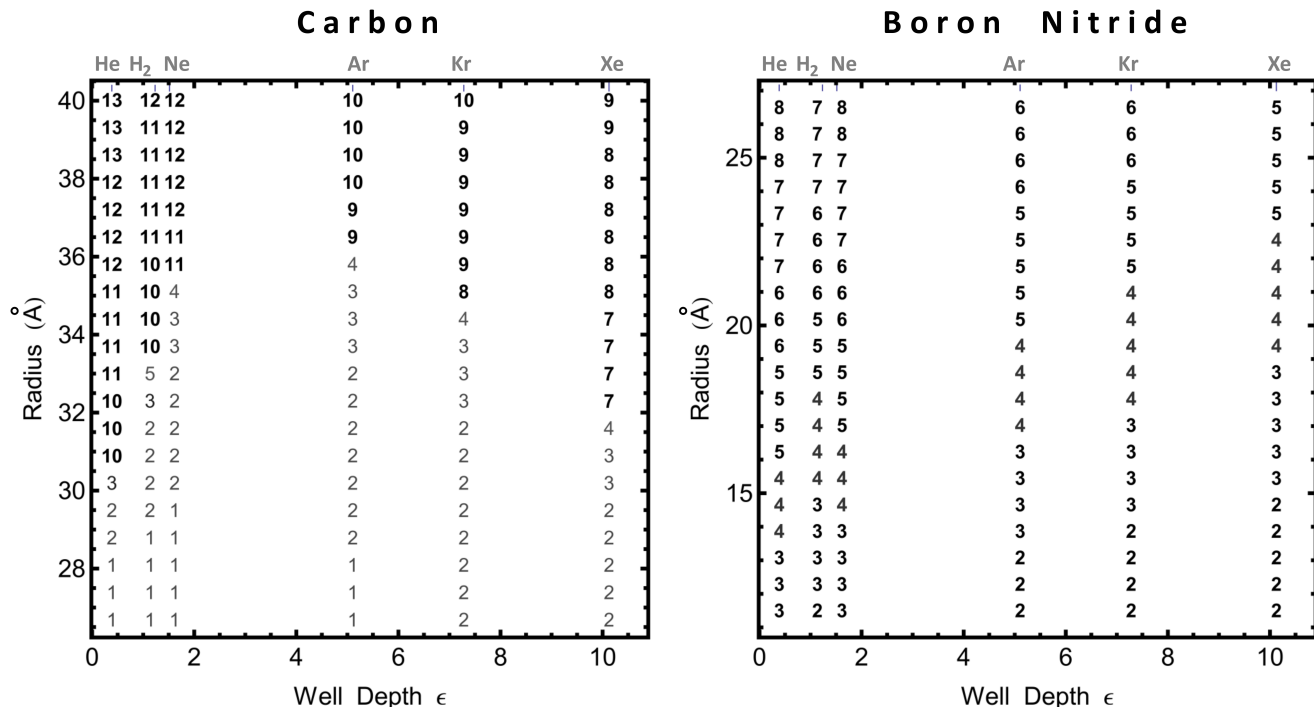


FIG. 7: The number $m(\epsilon, D)$ of shells formed in the expanded region of carbon and boron-nitride tubes during the initial expansion $\mathbf{C1} \rightarrow \mathbf{Em}$. Bold font indicates a transition directly into a fully filled pore: capillary condensation simultaneous with shape transition. The bottom of the range of radii shown corresponds to R_t , the size at which collapse becomes energetically favorable. ϵ is given in units of ϵ_C .

case of a wide, single-layer sp^2 carbon pore, but the phenomena are general to any thin-walled geometry that can change its shape in a bistable manner through variation in mean curvature and interfacial contact. For example, boron nitride nanotubes have lower elastic stiffness ($0.0275 \text{ eV } \text{Å}^2/\text{atom}$ versus $0.0405 \text{ eV } \text{Å}^2/\text{atom}$ for carbon²⁹) and larger interfacial energies ($\epsilon_{BN} = 5.08 \cdot 10^{-3}$ versus $\epsilon_C = 2.39 \cdot 10^{-3}$), thus they cross over to favor collapse at a much smaller pore radius, as depicted in Fig. 11 of the Appendix. The gas-tube interaction energy of Eqn. (1) increases relative to that for carbon, due to the larger values of ϵ_W that enter the combining rules. The right panel of Fig. 7 shows the resulting sequence of expanded shell phases for the BN system. Since the crossover radius R_t is much smaller, gas atoms adsorbed in the expanded region coordinate more strongly to the pore walls, thus making the coupling of pore expansion to capillary condensation particularly strong. The $\mathbf{C1} \rightarrow \mathbf{Em}$ transition always occurs at the maximal shell number m consistent with the boron nitride pore radius.

III. SUMMARY AND CONCLUSIONS

Employing a lattice gas model, we have investigated shape transformations between collapse and expansion driven by adsorbed gas in pores with atomically thin,

flexible walls as could be produced by a wide range of emerging two-dimensional materials, when wrapped into suitable pore geometries. Narrow-enough tubes are always expanded and simply form sequences of absorbed concentric shells as the gas chemical potential increases. Wider tubes without gas are most stable when collapsed, but can be expanded when connected to a gas reservoir, with one or more concentric shells adsorbed on the inner surface of the expanded region. This inflation is driven not by the pressure of a bulk vapor phase, but by the increased surface area for adsorption liberated by lifting apart the opposing faces of the collapsed pore. The number of concentric shells formed at the threshold chemical potential for expansion depends on gas-gas interactions, gas-substrate interactions, and pore radius. For a fixed number of gas atoms, the system can also assume a mixed state with partial collapse and partial expansion. The precise conditions for these transitions are sensitive to the detailed parametrization of the interaction potentials (and potential inclusion of quantum effects for the lightest gases), but the overall behavior of these shape-changing pores is generic and robust.



FIG. 8: Periodic (in axial direction) unit cells of (40,40) collapsed and expanded tube configurations. Similar cells of different diameter tubes were used for computations of per unit length energies U_- , U_+ , and difference $\Delta U = U_+ - U_-$ shown in Fig. 3.

IV. ACKNOWLEDGMENTS

We thank Alex Archer for valuable discussions and acknowledge NSF CMMI-0727890, DMR-0707332 and U.S. Army Research Office MURI grant W911NF-11-1-0362 for support.

V. APPENDIX: ATOMISTIC SIMULATION

A. Elastic energy of the tube wall

Molecular dynamics simulations with the LAMMPS¹⁹ packaged were used to calculate the energy per unit of nanotube length for the empty expanded (U_+) and collapsed (U_-) configurations shown in Fig. 8. The bonded and non-bonded inter-carbon interactions were modeled with an adaptive intermolecular reactive empirical bond order (AIREBO) potential²⁰. Energies were computed for armchair nanotubes of different radii R after corresponding unit cells were relaxed (at zero temperature) with periodic boundary conditions. The resulting radius dependence of $\Delta U(R) = U_+(R) - U_-(R)$ for a pure-carbon sp² pore wall is shown in Fig. 3.

B. Low temperature molecular dynamics simulations

To validate the structures of the gas shells absorbed inside the tube that were used in our zero-temperature approach, we performed representative low-temperature molecular dynamics simulations of a carbon nanotube with a fixed number of helium atoms inside. Initially, an empty 900Å long (44,44) single-wall carbon nanotube was relaxed with one end fixed in the expanded state and

the other in the collapsed state. Similar to the top image in Fig. 1, this empty tube is mostly collapsed. 11200 helium atoms were then arranged inside the expanded part of the nanotube, both ends of which were sealed by potential barriers to prevent gas from exiting the tube. Using a Nose-Hoover thermostat, the system was initially heated to 100 K for several hundred ps, so that the helium could wet the accessible area inside the tube. The system was then cooled and equilibrated at 10 K for 400 ps. Examples of equilibrium configurations are shown in Fig. 1. A face-on view of exactly half of the system – collapsed at the top and expanded at the bottom – is shown in Fig. 9a. Figs. 9d and e show one fully formed closed-packed gas shell and a second partially filled shell inside the expanded segment of the tube. Figs. 9b and c show a segment of the collapsed region of the tube with a single closed packed shell in the bulb. (For clarity, each view shows exactly one-half of the full structure). Defects in the closed-packed structure of the shell may result from either finite temperature effects, incomplete system equilibration due to slow dynamics at low temperature, or the fixed number of gas atoms being incommensurate to the number required to form a completed shell in this finite-length system. Since the center-to-center distance between opposing gas atoms in the bulb ($\sim 4\text{\AA}$) is significantly smaller than twice the equilibrium distance between gas atoms ($\sim 6\text{\AA}$), the formation of a second shell in the bulb is highly suppressed, and such a shell can be populated only at high temperatures that are beyond the scope of our study. Gases heavier than helium would require larger inter-shell equilibrium distances, making formation of second shell in the bulb at low temperature even less likely.

VI. APPENDIX: SIMPLIFIED ELASTIC MODEL

A brief analysis given here establishes the parameters of mechanical bistability needed to analyze systems with walls composed of hexagonal boron nitride, following a method similar to that used previously^{3,5}. Taking the curvature-dependent elastic strain energy density²⁹ $U_+^e = C/2R^2$ to be a function of local radius R , the energy per axial unit length of the expanded tube is $U_+ = \pi C/R$ (measured relative to the energy of formation of the elastic sheet). The D_2 dihedral symmetry of the collapsed tube's cross-section allows its shape to be described by measuring arc lengths within one quarter of the cross-section, as shown in Fig. 10. a is a half of the flat region where two walls come in contact; r is the radius of the bulb; and $l = \pi R/2 - a$ is the length of the non-contacted region, a portion $b = l - \pi r/2$ of which forms the non-circular part of the bulb. The energy density U_- of the collapsed tube consists of the strain elastic energy $U_-^{er} = \pi C/r$ of two bulb regions of total length $2\pi r$; the strain elastic energy U_-^{eb} together with a non-bonded interlayer energy U_-^{vb} in four transition tube segments of length b each; and a non-bonded interlayer attraction between the walls in the flat middle regions of width $2a$.

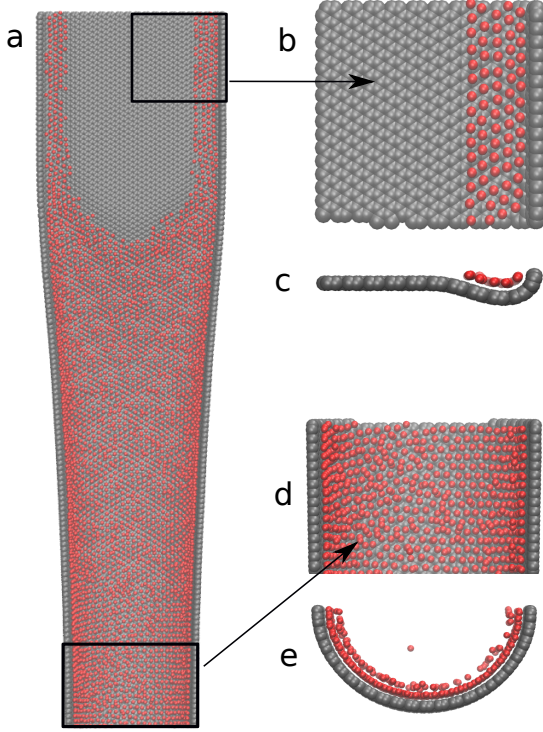


FIG. 9: (Color online) Shell structures of helium (red) absorbed inside a (44,44) carbon nanotube (gray) at $T = 10\text{K}$. The portion of the system closest to the viewer is removed for clarity, to expose the interior. (a) Longitudinal view showing the interior of the tube and the transition between collapse (top) and expansion (bottom). Fig. 1 shows a side view of a similar system. (b) Close-up of the collapsed region, showing a close-packed single shell of helium absorbed in the bulb. The gray area is the region where the opposing tube walls are in direct contact. (c) Side view of single shell in the bulb. (d) Close-up of the expanded region with close-packed gas shells. (e) Gas is absorbed into two shells with the second one being incomplete.

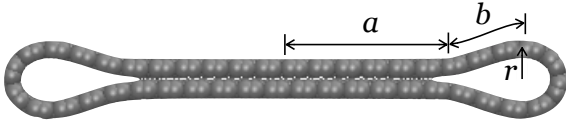


FIG. 10: Schematic showing geometric parameters of the collapsed tube cross-section. $2a$ is the width of the collapsed region; b is the length of the non-contacted wall part. r is the radius of the bulb region.

The last energy can be approximated using the interac-

tion energy density of two infinite flat sheets:

$$U_{\text{sheet}}(d) = 8\epsilon\pi\theta^2 \int_0^\infty \left[\left(\frac{\sigma}{\sqrt{r^2 + d^2}} \right)^{12} - \left(\frac{\sigma}{\sqrt{r^2 + d^2}} \right)^6 \right] r dr \quad (8)$$

$$= 2\pi\epsilon\theta^2\sigma^6(2\sigma^6 - 5d^6)/(5d^{10}).$$

Here $\theta = 0.38 \text{ \AA}^{-2}$ is the areal density of atoms in one sheet; ϵ, σ are the Lennard-Jones well depth and the zero-potential distance. Minimization of $U_{\text{sheet}}(d)$ with respect to inter-sheet distance d provides equilibrium spacing d_0 . Therefore, the interaction energy per unit axial length of the central flat tube region of width $2a$ is $U_{-}^{va} \approx 2aU_{\text{sheet}}(d_0)$. Linear plate theory yields the elastic strain energy in each out of four transition regions of length b as

$$U_{-}^{eb} = \frac{6C}{(l - \pi r/2)^3} \left(r - \frac{d_0}{2} \right)^2. \quad (9)$$

The non-bonded interlayer energy associated with the same region of length b is approximated by the averaged value $U_{-}^{vb} = b[U_{\text{sheet}}(d_0) + U_{\text{sheet}}(2r)]/2$. Using dimensionless parameters $\alpha = \pi r/2l$ and $\beta = d_0/2l$, the tube energy per axial unit length becomes

$$U_{-} = 4U_{-}^{eb} + U_{-}^{er} + U_{-}^{va} + 4U_{-}^{vb}$$

$$= \frac{24C}{l(1 - \alpha)^3} \left(\frac{2\alpha}{\pi} - \beta \right)^2 + \frac{\pi^2 C}{2\alpha l}$$

$$+ (2l - \pi R)U_{\text{sheet}}(d_0)$$

$$+ 2(l - \alpha l)(U_{\text{sheet}}(d_0) + U_{\text{sheet}}(2r)). \quad (10)$$

The system of equations $a = \pi R/2 - l$, $b = l - \alpha l$, $\partial U_{-}/\partial l$, and $\partial U_{-}/\partial \alpha$, solved for a , b , α , and l , determines the shape of the collapsed tube. Assuming that shape of the transition region of length b does not depend on the tube size R , the corresponding term $4U_{-}^{vb}$ can be omitted during the shape determination but retained for the calculation of the energy U_{-} . The energy difference

$$\Delta U(R) = U_{\circ} - U_{-} \quad (11)$$

between expanded and collapsed shapes is shown with black and orange lines in Fig. 11 for carbon and boron-nitride walls respectively. For comparison, the blue line shows the results of molecular dynamics relaxation of an atomistic model of an armchair tube with the same radius – the deviation between these two treatments of carbon gives a sense of the level of approximation involved in the simplified continuum model. We take²⁹ $C_C = 4.05 \text{ eV \AA}^2/\text{atom}$ and $C_{BN} = 2.75 \text{ eV \AA}^2/\text{atom}$ and use Lennard-Jones parameters²³ $\epsilon_C = 2.39 \cdot 10^{-3} \text{ eV}$ and $\sigma_C = 3.41 \text{ \AA}$. The boron-nitride parameters are obtained through the combining rules $\epsilon_{BN} = \sqrt{\epsilon_B \epsilon_N}$ and $\sigma_{BN} = (\sigma_B + \sigma_N)/2$,

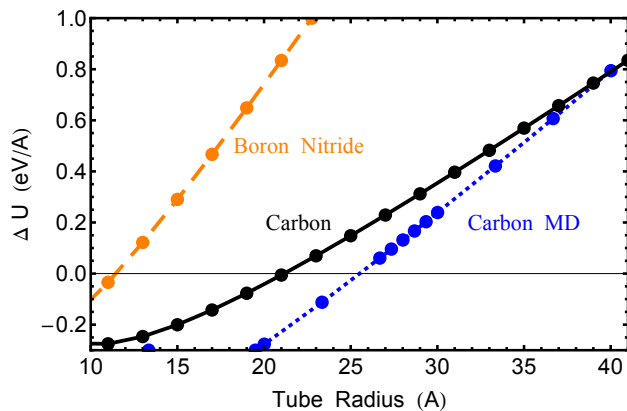


FIG. 11: (Color online) The difference in energy per unit length $\Delta U(R) = U_o - U_-$ between the expanded (U_o) and collapsed (U_-) configurations for an empty tube. The blue line shows results of molecular dynamics simulations; the black and orange lines show $U(R)$ results from the simplified continuum model of Eqn. (11). The collapsed shape minimizes the energy for tubes with radius R for which $\Delta U(R) > 0$.

where boron and nitrogen values of $\epsilon_B = 4.116 \cdot 10^{-3}$ eV, $\sigma_B = 3.453$ Å, and $\epsilon_N = 6.281 \cdot 10^{-3}$ eV, $\sigma_N = 3.365$ Å are from a continuum analysis of hexagonal BN systems³⁰.

- ¹ R. A. Trasca, M. M. Calbi, and M. W. Cole, Phys. Rev. E. **65**, 061607 (2002).
- ² N. G. Chopra, L. X. Benedict, V. H. Crespi, M. L. Cohen, S. G. Louie, A. Zettl, Nature **377**, 135 (1995).
- ³ L. X. Benedict, V. H. Crespi, N. G. Chopra, A. Zettl, M. L. Cohen, S. G. Louie, Chem. Phys. Lett. **286**, 490 (1998).
- ⁴ G. Gao, T. Cagin, W. A. Goddard, Nanotechnology **9**, 184 (1998).
- ⁵ T. Tang, A. Jagota, C.-Y. Hui, N. J. Glassmaker, J. Appl. Phys. **97**, 074310 (2005).
- ⁶ S. Zhang, R. Khare, T. Belytschko, K. J. Hsia, S. L. Mielke, G. C. Schatz, Phys. Rev. B **73**, 075423 (2006).
- ⁷ E. Mockensturm, A. Mahdavi, V. Crespi, Proc. of IMECE 2005, 82991 (2005).
- ⁸ O. E. Shklyaev, E. Mockensturm, V. H. Crespi, Phys. Rev. Lett. **106**, 155501 (2011).
- ⁹ T. Chang, Z. Guo, Nano Lett. **10**, 3490 (2010).
- ¹⁰ O. E. Shklyaev, E. Mockensturm, V. H. Crespi, Phys. Rev. Lett. **110**, 156803 (2013).
- ¹¹ J. Kou, X. Zhou, Y. Fang, Y. Chen, H. Lu, H. Ye, F. Wu, and J. Fan, Appl. Phys. Lett. **102**, 123902 (2013).
- ¹² F. Ancilotto, M. W. Cole, A. Grosman, E. S. Hernandez, F. Toigo, J. Low Temp. Phys. **163**, 284 (2011)
- ¹³ H.-Y. Kim, S. M. Gatica, G. Stan, M. W. Cole, J. Low Temp. Phys. **156**, 1 (2009)
- ¹⁴ These mechanical boundary conditions are needed in the case of an unfilled tube (i.e. in the absence of gas) to enable the system to surmount the activation barrier between expanded and collapsed states. It is possible that gas-mediated shape transitions have lower barriers, since the gas can fill the partially expanded intermediate shape.
- ¹⁵ G. Vidali, M. W. Cole, J. R. Klein, Phys. Rev. B **28**, 3064 (1983).
- ¹⁶ G. Stan, M. J. Bojan, S. Curtarolo, S. M. Gatica, M. W. Cole, Phys. Rev. B **62**, 2173 (2000).
- ¹⁷ M. M. Calbi, S. M. Gatica, M. J. Bojan, G. Stan, M. W. Cole, Rev. Mod. Phys. **73**, 857 (2001).
- ¹⁸ M. J. De Oliveira and R. B. Griffiths, Surf. Sci. **71**, 687 (1978).
- ¹⁹ S. Plimpton, J. Comp. Phys. **117**, 1-19 (1995) (<http://lammps.sandia.gov>)
- ²⁰ S. Stuart, A. Tutein, J. Harrison, J. Chem. Phys. **112**, 6472 (2000).
- ²¹ Z. J. Han and K. Ostrikov, J. Am. Chem. Soc. **134**, 6018 (2012).
- ²² G. Stan, M. W. Cole, Surf. Sci. **395**, 280 (1998).
- ²³ L. A. Girifalco, M. Hodak, R. S. Lee, Phys. Rev. B **62**, 13104 (2000).
- ²⁴ I. F. Silvera, Rev. Mod. Phys. **52**, 393 (1980).
- ²⁵ M. Hodak, L. A. Girifalco, Phys. Rev. B. **67**, 075419 (2003).
- ²⁶ S. B. Legoas, R. P. B. dos Santos, K. S. Troche, V. R. Coulucci, D. S. Galvao, Nanotechnology **22**, 315708 (2011).
- ²⁷ Y. J. Dappe, J. Phys. D: Appl. Phys. **47**, 083001 (2014).
- ²⁸ S. M. Gatica, G. Stan, J. K. Johnson, M. W. Cole, J. Low Temp. Phys. **120**, 337 (2000)
- ²⁹ E. Hernandez, C. Goze, P. Bernier, A. Rubio, Appl. Phys. A **68**, 287-292 (1999)
- ³⁰ N. Thamwattana and J. M. Hill J. Phys.: Condens. Matter **19**, 406209 (2007).